APPLIED SCIENCES AND ENGINEERING

3D printing of a wearable personalized oral delivery device: A first-in-human study

Kun Liang,* Simone Carmone, Davide Brambilla,† Jean-Christophe Leroux‡

Despite the burgeoning interest in three-dimensional (3D) printing for the manufacture of customizable oral dosage formulations, a U.S. Food and Drug Administration–approved tablet notwithstanding, the full potential of 3D printing in pharmaceutical sciences has not been realized. In particular, 3D-printed drug-eluting devices offer the possibility for personalization in terms of shape, size, and architecture, but their clinical applications have remained relatively unexplored. We used 3D printing to manufacture a tailored oral drug delivery device with customizable design and tunable release rates in the form of a mouthguard and, subsequently, evaluated the performance of this system in the native setting in a first-in-human study. Our proof-of-concept work demonstrates the immense potential of 3D printing as a platform for the development and translation of next-generation drug delivery devices for personalized therapy.

INTRODUCTION

Additive manufacturing, or three-dimensional (3D) printing as it is commonly known, has developed at an impressive pace in recent years, revolutionizing the prototyping and manufacturing processes across many industries including sectors such as automotive, aerospace, and medicine (*1*–*4*). In the pharmaceutical field, 3D printing could allow novel drug delivery systems to be manufactured with unprecedented complexity and precision, achieving detailed spatial composition and controllable release patterns not feasible (or difficult to achieve) with conventional formulation techniques (*5*–*7*). The speed and flexibility of 3D printing also propel health care closer toward the goal of personalized medicine, enabling the on-demand, on-site manufacturing of customizable products to fit patient-specific needs (*8*, *9*). Most advances made in this direction have so far concerned simple oral dosage forms (that is, tablets), where single or combinations of multiple drugs were incorporated and spatial and temporal control over drug release were demonstrated through adjustments in polymer content (*10*, *11*), geometry (*12*), compartmentation (*13*, *14*), or infill pattern (*15*, *16*). The recent U.S. Food and Drug Administration approval of the first 3D-printed rapidly orodispersible tablet of an antiepileptic drug has set the precedent for these systems (*17*). We foresee that the contributions of 3D printing can go well beyond the production of complex tablets, fabricating, for instance, personalized wearable/implantable devices with sustained drug release capability (*18*–*20*), where the exclusive advantage of material shaping conferred by 3D printing can be fully exploited. In this scenario, additive manufacturing can be coupled with 3D scanning technology that captures information about the patients' anatomical features to produce a tailored device that precisely fits the size and geometric requirements. There have been recent research efforts exploring 3D scanning and printing of drug-laden patches that tailor to patient-specific anatomic features such as the nose (*21*, *22*). Nevertheless, the transition of 3D-printed drug delivery devices from the laboratory to the clinic remains a monumental challenge. A primary reason for the gap between prototyping and application is that, although ample progress has been made in 3D printing technologies, the materials and standardized procedures remain generally inadequate from a pharmaceutical perspective, hampering the development of consistent, scalable, 3D-printed drug-eluting devices (*8*, *23*, *24*). To our knowledge, no studies have assessed the performance and drug release of a 3D-printed device in the native setting, that is, worn or implanted in humans.

Here, we report the establishment of a systematic, well-defined, iterative process of printable material development, 3D prototype design and in vitro characterization, and the first-in-human study of a 3D-printed wearable oral delivery device (Fig. 1) in the form of a mouthguard. The mouthguard, a widely used device for dental protection or alignment, was chosen as a proof-of-concept oral delivery device to exploit the shape customizability endowed by 3D printing. Personalized mouthguards, which can be 3D-printed on the basis of dentition impressions obtained from individualized intraoral scans, can deliver a preloaded compound in the oral cavity. In particular, oral diseases can be treated by the local sustained release of a drug from the mouthguard. Chlorhexidine-coated mouthguards have previously been tested in humans for the suppression of oral bacteria (*25*). Here, clobetasol propionate (CBS) was selected as the model drug because it is an effective topical drug for alleviating oral inflammation, for example, lichen planus (*26*). For the human release study, it was replaced with the food-grade flavor vanillic acid (VA). From the various 3D printing technologies, we selected fused deposition modeling (FDM), a technique in which molten thermoplastic is deposited on a print bed to build up objects in a layer-by-layer manner (*27*), because this manufacturing process does not require organic solvents or toxic photoactive resins, thus circumventing potential health risks or other obstacles for clinical applications (*23*, *28*). To facilitate clinical translation, we selected unmodified poly(L-lactic acid) (PLA) and poly(vinyl alcohol) (PVA) as the thermoplastic polymers because they are commonly used in FDM and pharmaceutical grades of these polymers are readily available for clinical applications. On the basis of these two polymers, we manufactured three types of mouthguards differing in terms of design or material composition and evaluated them in human volunteers for their suitability as drug delivery devices. This work demonstrates a 3D-printed tailored sustained delivery device in human that allows for full customizability in terms of tunable release and design, marking an important step in bridging the gap between modeling and clinical application of 3D-printed drug delivery devices.

Department of Chemistry and Applied Biosciences, Institute of Pharmaceutical Sciences, ETH Zürich, Zürich, Switzerland.
*Present address: Institute of Bioengineering and Nanotechnology, 31 Biopolis Way, The Nanos, Singapore 138669, Singapore.
†Present address: Faculty of Pharmacy, University of Montreal, H3T 1J4 Montreal, Quebec, Canada.
‡Corresponding author. Email: jleroux@ethz.ch

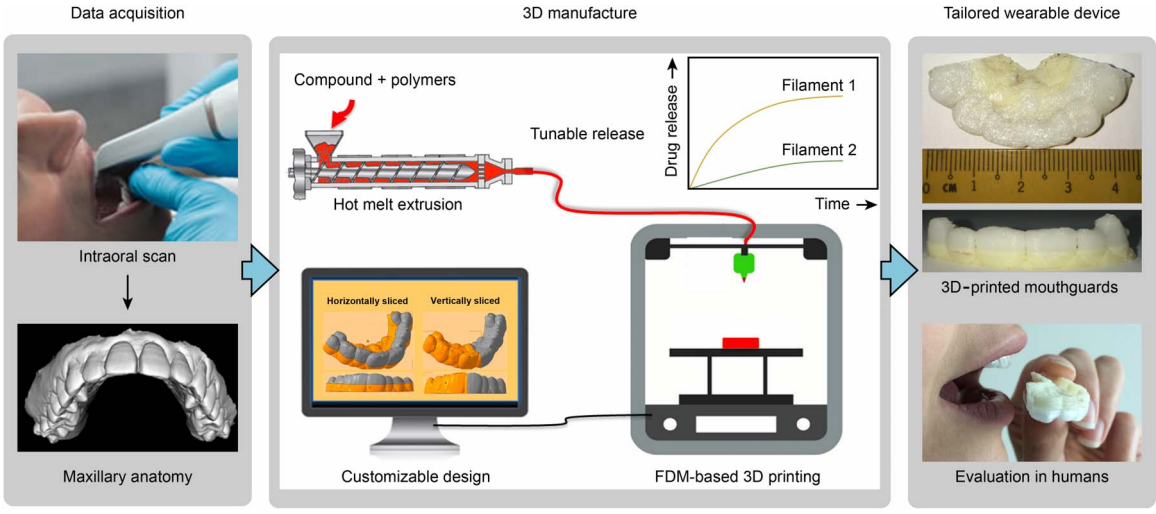

Fig. 1. Workflow for the manufacture of wearable personalized oral delivery mouthguards by 3D printing. The manufacture of personalized oral delivery mouthguards by 3D printing involved two stages. In the data acquisition stage, we obtained an intraoral scan of the maxillary anatomy of the subject and the impression served as the template for 3D printing. 3D manufacture began with the production of printable pharmaceutical-grade (PG) filaments loaded with the desired compound by hot melt extrusion (HME). We obtained filaments with tunable release rates by adjusting the polymer composition in the feed and subsequently used them to fabricate prototypes with customizable designs (based on the scanned templates) by FDM-based 3D printing. Finally, we evaluated the performance of the personalized 3D-printed mouthguard on each individual.

RESULTS

Material selection and filament production

Fabrication of the prototypes was a two-step process. First, we subjected various blends of PLA and PVA plus either CBS or VA to HME to produce filaments with tunable release kinetics. We then used these filaments as feedstocks for FDM printing. We selected CBS, an anti-inflammatory corticosteroid, as a model drug, with VA, a food-grade flavor substitute, as the model active compound for the first-in-human study (Fig. 2A). Although the physicochemical properties of these two compounds differ significantly (table S1), they were suitable because of their thermal stability against the high temperatures used in the HME (150° to 190°C) and FDM (180° to 195°C) processes. Thermogravimetric analysis (TGA) revealed weight losses of 0.13 and 9.6% at temperatures up to 195°C for CBS and VA, respectively (Fig. 2B). Although there was some degradation of VA, it exhibited higher thermal stability than other tested food-grade flavors (fig. S1A).

The chosen feed concentrations of CBS [10 weight % (wt %)] and VA (2.5 wt %) were the highest attainable concentrations that yielded consistent filaments usable for printing. Hot melt extruded filaments loaded with either CBS or VA were produced using two optimized PVA/PLA feed weight ratios. These ratios were applied either to standard PLA_S, standard PVA_S, and CBS or to PG PLA_{PG}, PG PVA_{PG}, and VA. PVA (high) and PVA (low) denote PVA/PLA feed weight ratios of 6:3 and 5:4 for CBS and 2:3 and 1:3 for VA, respectively. The PG polymers were used to produce VA-loaded filaments for the first-in-human study.

All filaments were cylindrical and exhibited relatively consistent diameters of 1.65 ± 0.1 mm (fig. S1B). For both PVA (high) and PVA (low), the loading efficiencies (amount of compound incorporated as a percentage of the amount in feed) were greater for VA (>85%) than for CBS (~60%) (Fig. 2C). Although a reduced PVA_S/PLA_S ratio led to a concomitant increase in loading efficiencies for CBS-containing filaments (table S2), filaments below a PVA_S/PLA_S ratio of 5:4 were not further evaluated, owing to the slow CBS release (less than 6% after 14 days) accompanied by the small weight reduction after dissolution (fig. S2).

An in vitro dissolution study (Fig. 2D) revealed that CBS was released in a sustained manner over 2 weeks from both PVA (high) and PVA (low) filaments, with the former exhibiting a higher cumulative release (39%) than the latter (19%). In contrast, a much quicker release of VA was observed for the PVA (high) filament, attaining 96% in 10 days, whereas only 2% of the VA was released from the PVA (low) filament (Fig. 2E). The higher hydrophilicity of VA could be responsible for the faster release of VA compared with CBS from the PVA (high) filaments. It was likely distributed preferentially in the PVA phase, which readily dissolved in the buffer, whereas the hydrophobic CBS was localized more predominantly in the PLA phase, which degraded slowly by hydrolysis. The miscibility analysis confirmed this finding, for which we performed solubility parameter calculations. Research has shown that, if the difference in the solubility parameter (δ) values between two substances is less than 5 $(MJ/m^3)^{1/2}$, then the two substances are miscible and interact favorably (*29*). As shown in table S3, only the CBS-PLA and VA-PVA pairs showed differences in solubility parameter values that were less than 5 $(MJ/m^3)^{1/2}$, indicating the enhanced miscibility of CBS in the PLA phase and of VA in the PVA phase.

The PVA (high) filaments exhibited greater weight loss compared with the PVA (low) counterparts for both compounds (Fig. 2F) after dissolution. The minimal weight loss observed in the VA-loaded PVA (low) filament (<2.5%), which was probably attributable to the retardation of PVA dissolution by the excess PLA, corresponded to the slow VA release in the dissolution study. Overall, we attained tunable release of both CBS and VA from the filaments by varying the PVA/PLA feed weight ratios of the blends during the extrusion process.

Filament characterization

We examined the physicochemical properties of the filaments before 3D printing and characterized thermal properties of the filaments by TGA and differential scanning calorimetry (DSC). TGA revealed that both the CBS-loaded and VA-loaded filaments exhibited <1% weight loss at temperatures up to 200°C (fig. S3). This result indicates that

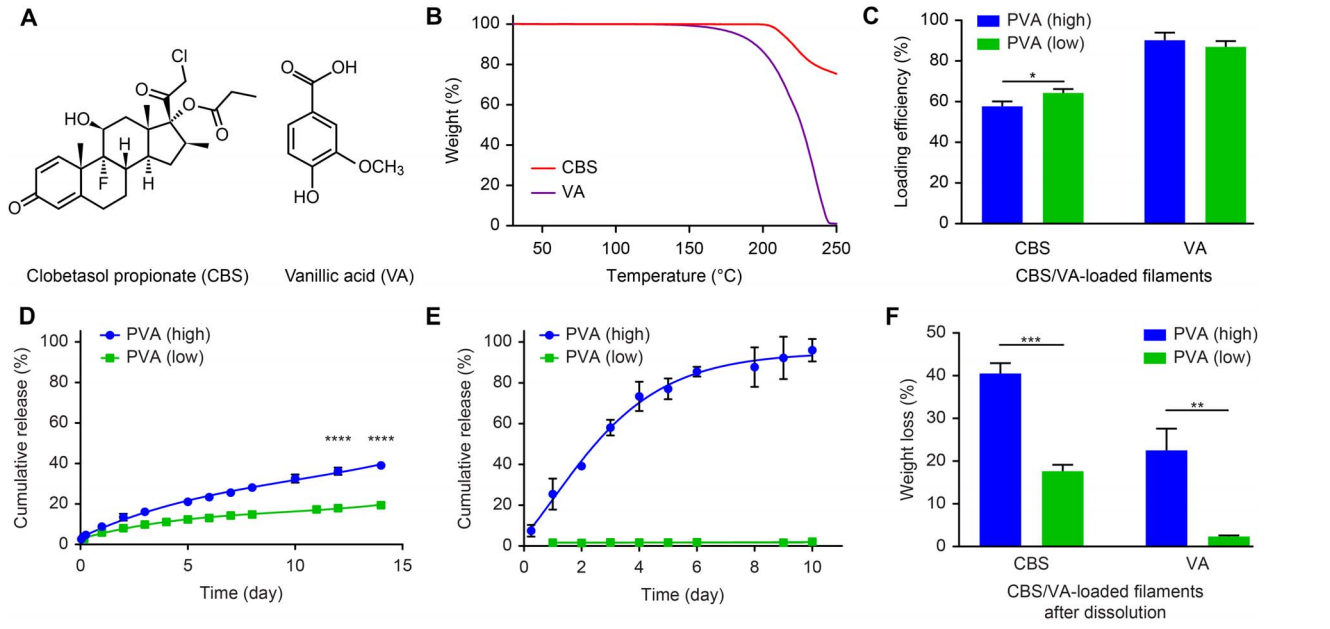

Fig. 2. Selection of compound-loaded filaments with tunable release properties for 3D printing. (**A**) Chemical structures of CBS and VA. (**B**) TGA thermograms of CBS and VA. (**C**) Loading efficiencies of CBS and VA in the filaments after HME. PVA (high) and PVA (low) represent PVA/PLA feed weight ratios of 6:3 and 5:4, respectively, for CBS and ratios of 2:3 and 1:3, respectively, for VA. (**D** and **E**) Cumulative release of the CBS-loaded (D) and the VA-loaded (E) filaments in vitro. (**F**) Weight loss of the CBS-loaded and VA-loaded filaments after the in vitro dissolution study. Data are means ± SD (n = 3). *P < 0.05, **P < 0.01, ***P < 0.001, and ****P < 0.0001.

the high thermal stability of these filaments makes them suitable for FDM printing. Although we detected the melting peak (T_m) of CBS (198°C) in the DSC thermograms of the powder mixtures before HME (fig. S4A), we did not observe any distinct T_m signal of CBS in the thermograms of the filaments (Fig. 3A), suggesting that CBS underwent an amorphous transformation after HME. The T_m peak of VA (212°C) was not observable in either the powder mixture or the filament (fig. S4B and Fig. 3B), possibly due to the lower proportion of VA in the feed. Furthermore, characteristic peaks corresponding to glass transition temperature (T_g) values of both PLA and PVA were visible in the DSC thermograms of the CBS-loaded filaments (Fig. 3A), indicating their immiscibility; this result is supported by the large difference in their solubility parameters (table S3). In comparison, only the T_g signal of PLA_{PG} was observable in the DSC thermograms of the VA-loaded filaments (Fig. 3B). The T_g peak of PVA_{PG} was indistinct, probably owing to the limited presence of amorphous domains in this grade of PVA (*30*).

We assessed the crystallinity of the compounds in the filaments further using x-ray powder diffraction (XRPD). The sharp diffraction peaks of crystalline CBS and VA between 10° and 30°, which were visible in the diffractograms of the powder mixtures (fig. S4, C and D), were absent in the diffractograms of the filaments (Fig. 3, C and D), confirming the amorphous dispersion of the compounds in the filament matrices. This result is consistent with previous reports of the amorphous transformation of crystalline drugs by dispersion in polymer matrices via HME (*31*, *32*).

Scanning electron microscopy (SEM) analyses of the internal microstructures of the filaments showed that for both the CBS-loaded and VA-loaded filaments, the external surface was rougher in PVA (high) than PVA (low) filaments (Fig. 3E). In addition, unlike the even texture of the cross sections observed for all unloaded polymer filaments (fig. S5), both the CBS-loaded and VA-loaded filaments appeared irregular, with prominent domains attributable to the various phases. This result indicates the incomplete solubility/miscibility of the compounds in the matrices.

The mechanical properties of the filaments, which were important predictors of their printability, were evaluated using texture analysis (TA). Filaments containing CBS displayed slightly lower tensile strengths of 47 to 49 MPa than both the pure PLA_S and pure PVA_S filaments (52 and 78 MPa, respectively) (Fig. 3F and table S4). The elongation at break (1.91 to 2.29%) was also reduced for the CBS-loaded filaments compared with the pure PLA_S (4.11%) and pure PVA_S (3.55%) filaments. We observed similar trends for the VA-loaded filaments, which exhibited tensile strengths in the range of 41 to 47 MPa compared with 60 MPa for pure PLA_{PG} and 71 MPa for pure PVA_{PG}. The elongation at break for VA-loaded filaments was also lower (3.34%) than that for PLA_{PG} (6.9%) and PVA_{PG} (5.11%) (Fig. 3G and table S5). Although we did not observe a reduction in tensile strength, studies have reported an increase in brittleness for other drug-loaded filaments (*33*, *34*). Overall, the similarity in the mechanical properties between the compound-loaded filaments and the pure PLA or PVA filaments indicated that the compound-loaded filaments would be suitable for FDM printing (*35*).

3D printing using CBS-loaded and VA-loaded filaments and evaluation of the prototypes

Before printing the mouthguards, we printed a model object (that is, a ring) to identify the optimal temperatures for 3D printing of the CBS-loaded and VA-loaded filaments, and we examined form and finishing of the rings, as well as the CBS and VA contents. The highest tested temperature (200°C) led to brown discoloration of the CBS-containing ring, and degradation of both CBS and VA occurred (fig. S6). In contrast, the lowest tested temperature (<180°C for CBS and <195°C for VA) led to incomplete prints, owing to poor melt viscosity and an uneven flow. Therefore, we chose printing temperatures of 180° and 195°C for CBS-loaded and VA-loaded filaments, respectively.

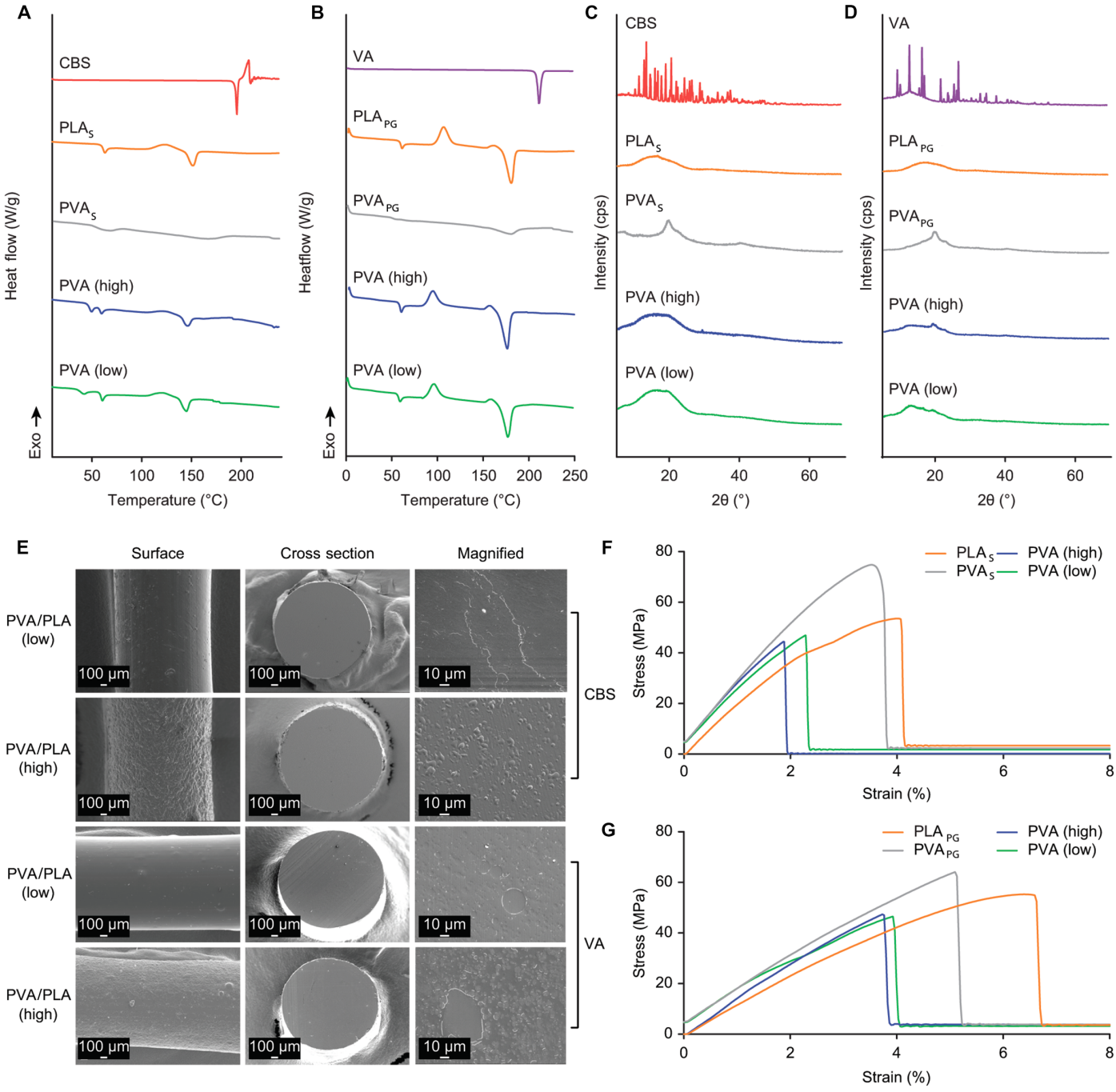

Fig. 3. Characterizations of filaments loaded with either CBS or VA. (**A** and **B**) DSC thermograms of pure CBS (A), filaments consisting of only PLA_S or PVA_S, CBS-loaded PVA (high), and PVA (low) filaments, and pure VA (B), filaments consisting of only PLA_{PG} or PVA_{PG}, as well as VA-loaded PVA (high) and PVA (low) filaments. (**C** and **D**) XRPD diffractograms of the same compounds and filaments as in (A) [for (C)] and (B) [for (D)]. (**E**) SEM images of filaments loaded with either CBS or VA: surface, cross section, and a magnified view of the cross section. Scale bars, 100 μm (for surface and cross section) and 10 μm (for a magnified view of the cross section). (**F** and **G**) Stress-strain curve of PLA_S, PVA_S, and CBS-loaded filaments (F) and PLA_{PG}, PVA_{PG}, and VA-loaded filaments (G).

An open-source model dental scan was used as a template to manufacture the 3D-printed mouthguards. To demonstrate the possibility of controlling the placement of the drug or flavor substitute for targeted release at different regions, we digitally modified the template by computer-aided design (CAD) software and sliced it horizontally into two regions: base and top, with or without the designated compound, respectively. We printed CBS-free top with commercial PLA filaments, but chose a filament comprising PLA_{PG}/PVA_{PG} (9:1, w/w) for the VA-free top because printing with the PLA_{PG} filament alone resulted in a high surface porosity (table S6). Figure 4 (A and B) shows the 3D-printed CBS-containing and VA-containing mouthguards, respectively, both of which exhibited a well-defined shape and form.

While more than 98% of the CBS remained in the mouthguards after printing, lower amounts of VA remained (89 to 91%), possibly due to degradation induced by the higher printing temperature used for the prototypes containing VA compared with those containing CBS (Fig. 4C).

The drug release kinetics of the printed mouthguards was evaluated by an in vitro dissolution assay. We observed and sustained release of CBS for both PVA (high) and PVA (low) CBS-loaded mouthguards over 14 days, with cumulative release values of 34% for the PVA (high) mouthguard versus 22% for the PVA (low) mouthguard (Fig. 4D). In comparison, VA released rapidly in the PVA (high) mouthguard, reaching 71% in 10 days, whereas the release in the PVA (low) mouthguard plateaued after 2 days at approximately 13% (Fig. 4E). These findings were consistent with the general trends seen in the release profiles of the CBS-loaded and VA-loaded isolated filaments (Fig. 2). Whitening of the regions containing the compounds accompanied the release of both compounds from the matrices of both types of mouthguards (Fig. 4F), which we believe could be due to the removal of PVA and compounds from the filament matrices by dissolution. We observed less weight loss and greater retention of the compounds in the PVA (low) mouthguards than in the PVA (high) counterparts (Fig. 4, G and H), in agreement with the corresponding release profiles. These results demonstrate the practicability of printing customizable mouthguard prototypes using the CBS-loaded and VA-loaded filaments, and implementing tunable release properties of the filaments (which were not affected by the printing process) in the prototypes.

Evaluation in human volunteers

We examined the feasibility of tailor-fitting VA-eluting mouthguards in six volunteers. First, we obtained the maxillary anatomical imprints of each individual using an intraoral scanner and subsequently digitally optimized them using them as templates for 3D printing of personalized mouthguards. Movie S1 illustrates the entire workflow for the manufacture of these mouthguards.

To demonstrate customizability in terms of VA locality and release kinetics, we manufactured three different types of personalized mouthguards by 3D printing using the VA-loaded filaments: horizontally sliced PVA (high) (HSPH), vertically sliced PVA (high) (VSPH), and horizontally sliced PVA (low) (HSPL) (Fig. 5A). The tailored mouthguards exhibited minimal loss (<10%) of VA content after printing and were fitted to each individual's maxillary anatomy (Fig. 5B). For the clinical trial, each volunteer wore each of the three types of mouthguard for 2 hours continuously per day over three consecutive days, with a 1-week break between each mouthguard test. The total wearing duration of 6 hours was chosen to simulate the likely application of such a device during sleep, which would minimize hindrances to daily tasks such as eating or drinking. We collected samples at 30-min intervals during each 2-hour cycle of wear, and quantified the VA concentrations in the saliva.

Figure 5C shows the VA concentrations in the saliva of the volunteers during the first cycle. Higher VA concentration was evident in both the HSPH and VSPH groups compared with the HSPL group at all time points, whereas there was no significant difference between the HSPH and VSPH groups. A similar trend appeared in the second cycle, although there was more VA in saliva in the HSPH than in the VSPH group at 30 and 120 min (Fig. 5D).

The higher saliva VA concentrations in the HSPH and VSPH groups led to a more than twofold enhancement in the area under the saliva VA concentration versus time curve [area under the curve (AUC)] compared with HSPL in the first two cycles (table S7). We did not find any significant differences between the three groups in terms of both saliva VA concentration and AUC in the third cycle (fig. S7A). We also observed gradual decline in saliva VA concentration over the three cycles for all three groups (note the change in the *y* axis scale between Fig. 5C and Fig. 5D), indicating a decline in the rate of VA release over time.

The weights of the mouthguards within each group decreased slightly (final weight loss, <10%) over time, but there was no significant difference across the three groups during the course of the trial (fig. S7B). The amount of VA that remained in the mouthguards of the HSPL group (78%) after the study was significantly higher compared with that of both the HSPH (39%) and VSPH (54%) groups (Fig. 5E), confirming the slower VA release in the HSPL group than in either the HSPH or VSPH group. Similar to the appearance observed after in vitro dissolution, a concomitant whitening of the VA-loaded regions of these mouthguards occurred after three cycles of wearing following the release of VA in the saliva (Fig. 5F).

To understand how the release of VA from the mouthguards in the native environment compared to the in vitro condition (Fig. 4, D and E), we performed a dissolution study for all three types of personalized mouthguards. The VA released from the HSPH, HSPL, and VSPH groups corresponded to the cumulative VA release in vitro at approximately 21, 57, and 19 hours, respectively (fig. S8)—considerably longer than the total wearing duration of 6 hours. The accelerated release of VA from the mouthguards in the mouth may be related to perturbations generated by constant tongue movements and intense salivation as a result of the continuous contact with the mouthguards. This behavior has also been reported for mucoadhesive patches (*36*).

DISCUSSION

We successfully manufactured a customizable oral delivery device, in the form of a mouthguard, by 3D printing. We produced filaments with tunable drug release profiles by varying the polymer composition in the matrices during HME production. In turn, we used these filaments as feedstock for the FDM-based 3D printing of prototypes with the same release properties. The tensile strengths of these filaments were comparable to the typical dental thermoplastics (5 to 60 MPa), whereas the elastic moduli were slightly higher than these materials (50 to 700 MPa) (*37*). However, the elongation at break (%) of the filaments was much lower than that of dental thermoplastics (>100% elongation). To improve the filament flexibility, ductile polymers such as poly(ethylene-vinyl acetate), which is already widely used for sport mouthguards (*38*), could be included in the blend in the future.

Following the optimization of the printing parameters for these filaments, the entire workflow from the intraoral scan to the final wearing of the customized VA-loaded mouthguard took less than 2 hours. Compared with conventional manufacturing techniques for standard mouthguards, such as casting and molding (*39*, *40*), this 3D printing fabrication process confers considerable advantages in terms of speed and efficiency and would enable manufacturing of these devices for immediate utilization. We anticipate that this approach could be readily replicated for the on-demand 3D manufacture of other personalized drug delivery devices, leading to a substantial reduction in waiting time for patients.

In volunteers, a sustained release of VA over the duration of wearing took place, with a comparable intervolunteer variability in saliva concentrations to other local drug delivery systems (*36*, *41*). In addition,

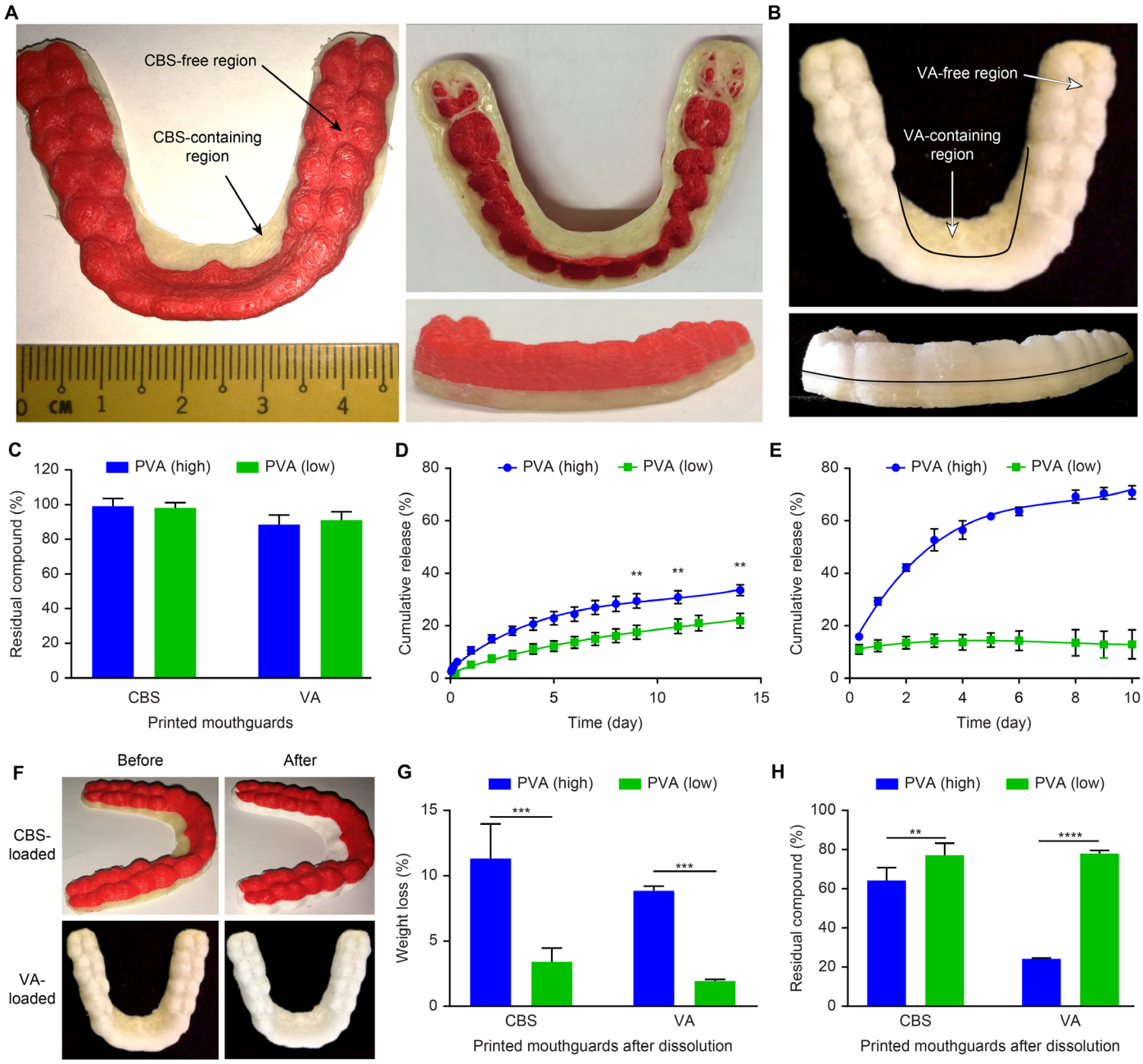

Fig. 4. 3D printing of mouthguards loaded with either CBS or VA that have tunable release properties. (**A**) Image of a 3D-printed mouthguard comprising a CBS-free top (red) and CBS-containing base (off-white) fabricated using PLA_S filament and PVA (high) CBS-loaded filament, respectively. (**B**) Image of a 3D-printed mouthguard comprising a VA-free top (white) and VA-containing base (off-white) fabricated using PLA_{PG}/PVA_{PG} (9:1, w/w) filament and PVA (high) VA-loaded filament, respectively. (**C**) Amount of residual CBS and VA in the mouthguards following 3D printing using the CBS-loaded and VA-loaded filaments. (**D** and **E**) Cumulative release of the CBS-loaded (D) and VA-loaded (E) mouthguards in vitro. (**F**) Images of the CBS-loaded and VA-loaded mouthguards before and after the in vitro dissolution study. A distinct whitening of the regions containing the CBS or VA occurred. (**G**) Weight loss of the CBS-loaded and VA-loaded mouthguards after the in vitro dissolution study. (**H**) Amount of residual CBS and residual VA in the mouthguards after the in vitro dissolution study. Data are means ± SD (n = 3). $^{**}P < 0.01$, $^{***}P < 0.001$, and $^{****}P < 0.0001$.

we found this variability to be relatively random. Hence, patient-specific factors, for example, salivating patterns, play a less important role in determining drug release from the mouthguard. From a clinical perspective, this would imply that patients wearing such a drug-eluting mouthguard would generally receive the desired dosage that the mouthguard is designed to administer. We noted that wearing the mouthguards led to some minor discomfort for the volunteers due to imperfect fitting and hindrance of speech. These issues were related to the low resolution of FDM manufacturing (nozzle diameter, ~350 μm) (*42*), which precluded the sculpting of well-defined, fine features and the building of thinner walls in the mouthguards. Several strategies could improve the resolution; for example, switching to a

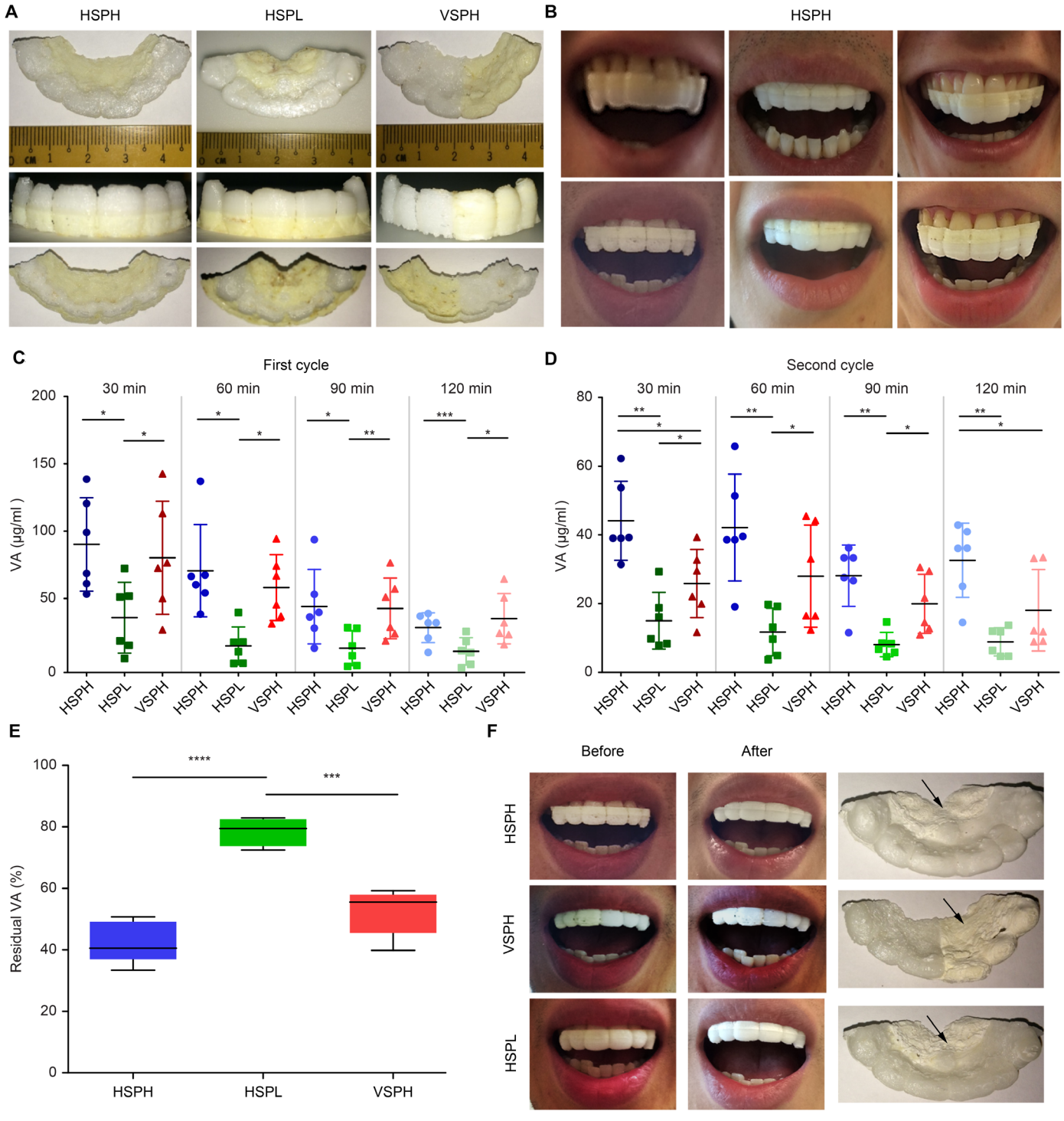

Fig. 5. 3D printing of tailored VA-loaded mouthguards for the first-in-human study and evaluation of VA release in the saliva. (**A**) 3D-printed VA-loaded mouthguards with three different designs: HSPH, VSPH, and HSPL. (**B**) Representative images of the 3D-printed VA-loaded mouthguards tailored to each volunteer's maxillary anatomy in the HSPH group. (**C** and **D**) Mean VA concentrations in the saliva of volunteers wearing mouthguards of the three designs during the first cycle (C) and second cycle (D) of wearing for 2 hours continuously. (**E**) Amount of residual VA in the mouthguards following three cycles of wearing by the volunteers. (**F**) Representative images of each of the three types of VA-loaded mouthguards before and after three cycles of wearing by the same volunteer. A distinct whitening of the region containing VA was observed, as indicated by the arrows. Data are means ± SD (n = 3). *P < 0.05, **P < 0.01, ***P < 0.001, and ****P < 0.0001.

microfabrication nozzle (*43*) or combining with an electric field–guided ink dispenser (*44*).

Here, we demonstrated the ability to incorporate CBS for the potential treatment of oral inflammation (*26*). Fluoride, a mineral routinely used for tooth decay prevention, is also an option. In particular, these mouthguards could overcome the issue of easy detachment of glass bead–type fluoride-releasing devices (*45*). Compared with conventional formulations of topical solutions or gels that are applied at high doses periodically, a drug-eluting mouthguard that releases the active compound over time would minimize washing away by saliva or overswallowing of drugs, thereby boosting treatment efficacy and reducing unwanted side effects. In addition, the possibility of controlling the locality of the drug-containing compartment in the mouthguard, as shown in this study, imparts spatial control over drug release, enabling preferential targeting of affected regions.

Moving forward, the use of other polymers commonly used in pharmaceutics, such as poly(ε-caprolactone) and poly(*N*-vinylpyrrolidone), with lower melting temperatures of 100° to 120°C (*18*, *46*), merit exploration for incorporating drugs with lower thermal stability. This would extend the applicability of this manufacturing process to include a large proportion of globally approved drugs, with melting temperatures of >100°C (*47*). In addition, because the release rate was controlled by the polymer composition in the filaments instead of by the design, geometry, or infill pattern, preservation of the shape, form, and integrity of the 3D-printed device should be feasible, offering the possibility of extending this 3D manufacturing process to other types of drug delivery devices, including stents and implants.

METHODS

Materials

Extrusion-grade PLA granulates [Ingeo 4043D; M_n = 143,000 Da, $Đ$ = 1.45, determined by gel permeation chromatography (GPC) measurements] were purchased from Resinex Switzerland AG, and PVA pellets (MOWIFLEX C 17; M_n = 66,000 Da, $Đ$ = 1.72, determined by GPC measurements) were provided by Kuraray Europe GmbH. CBS (molecular weight, 466.97) was obtained from Nutragreenlife Biotechnology Co. Phosphate-buffered saline (Gibco) was purchased from Thermo Fisher Scientific. PG polymers were used to manufacture the mouthguards for the human studies. PLA granulates [PURASORB PL 18, good manufacturing practice (GMP)–grade homopolymer of L-lactide; M_n = 147,000 Da, $Đ$ = 1.5) were purchased from Purac Biochem. PVA powder (Parteck MXP EMPROVE ESSENTIAL Ph. Eur, GMP-grade polymer; M_n = 75,000 Da, $Đ$ = 1.95, determined by GPC measurements) was provided by Merck KGaA. All food-grade flavor compounds, including VA, maltol, cinnamic acid, and ethyl vanillin, were purchased from Sigma-Aldrich.

HME of filaments

CBS-loaded or VA-loaded filaments for FDM printing were produced using single-screw extruders. First, the desired amount of PLA_S, PVA_S plus CBS or PLA_{PG}, PVA_{PG} plus VA at the indicated composition ratios (with a total weight of 40 g per batch) was physically mixed for 30 min with a TURBULA T2C shaker-mixer (Willy A. Bachofen AG Maschinenfabrik). Before preparing the mixture, the extrusion-grade PVA pellets were milled using a fine-mill machine (Typ MFC, CZ13, Culatti AG), whereas the PLA_{PG} was milled using a standard coffee milling machine (Melitta Molino, Melitta GmbH) to obtain finer granulates. Subsequently, the powder mixtures were processed by HME. CBS-loaded filaments were prepared using a Noztek Pro High Temperature extruder (Noztek) at a temperature of 145° to 150°C and a rotation speed of 15 rpm. VA-loaded filaments were prepared using a 3Devo Advanced Black single-screw extruder (3Devo) equipped with four separately regulated heating zones (H1, H2, H3, and H4) set at temperatures of 190°C (H1), 190°C (H2), 180°C (H3), and 170°C (H4). The extrusion speed was fixed at 8 rpm. The winder speed and puller speed were adjusted ad hoc to ensure that a constant filament diameter of 1.65 ± 0.1 mm was achieved.

Solubility parameter calculations

To estimate the miscibility of the compounds with the polymers, Hoftyzer and Van Krevelen group contribution methods (Eqs. 1 to 4) were used to calculate the solubility parameters of the compounds and polymers

$$\delta = \sqrt{\delta_d^2 + \delta_p^2 + \delta_h^2} \quad (1)$$

$$\delta_d = \frac{\sum F_{di}}{V} \quad (2)$$

$$\delta_p = \frac{\sqrt{\sum F^2{}_{pi}}}{V} \quad (3)$$

$$\delta_h = \sqrt{\frac{\sum E_{hi}}{V}} \quad (4)$$

where δ is the solubility parameter, F_{di} is the dispersion component of the molar attraction constant, F_{pi} is the polar component of the molar attraction constant, E_{hi} is the hydrogen-bonding energy component, and V is the molar volume. The V of CBS, VA, PLA, and PVA polymer repeat units was determined using the Fedors method (*29*).

The solubility parameters of the compounds and polymers were also calculated using the Hoy group contribution method (Eqs. 5 and 6)

$$\delta = \frac{\left(F_t + \frac{B}{n}\right)}{V} \quad (5)$$

$$n = \frac{0.5}{\Delta T} \quad (6)$$

where δ is the solubility parameter, F_t is the molar attraction function, B is the base value, n is the number of repeating units per effective chain segment of the polymer, ΔT is the Hoy correction for nonideality for polymers, and V is the molar volume. The final solubility parameters were obtained by taking the average of the two estimation methods (*10*, *29*).

Quantification of CBS and VA concentrations

The CBS or VA concentrations in the filaments and the printed prototypes were determined by high-performance liquid chromatography (HPLC). Before HPLC measurement, a section of the CBS-loaded or VA-loaded filament and the 3D-printed prototypes (approximately 10 mg) was placed in 500 μl of dimethyl sulfoxide and incubated in a shaker for 30 min at 90°C until complete dissolution. The solution was then diluted (1:20, v/v) using the HPLC mobile phase and assayed using a Dionex UltiMate 3000 Standard Dual HPLC system

(Thermo Fisher Scientific). Chromatographic separation was carried out on an XBridge C18 (250 mm × 4.6 mm, 5 μm) analytical column. The mobile phase consisted of acetonitrile and phosphate buffer (pH 3, adjusted with phosphoric acid; 14.7 M) (80:20, v/v) at an isocratic flow rate of 1 ml/min over a 5-min run time. The injection volume was 20 μl. The ultraviolet wavelengths of 241 and 270 nm were chosen to detect CBS and VA, respectively. A linear standard curve was obtained for CBS concentrations between 0.2 and 100 μg/ml and for VA concentrations between 0.25 and 100 μg/ml, respectively. All measurements were performed in triplicate.

Thermal analysis

The thermal behaviors of the CBS-loaded or VA-loaded filaments and the corresponding powder mixtures were investigated by TGA and DSC. For TGA analysis, TA Q50 TGA (TA Instruments–Waters LLC) was used. Approximately 10 mg of the samples was loaded onto aluminum pans and heated gradually from room temperature (approximately 24°C) to 300°C at 10°C/min. Nitrogen gas was used as a purge at a flow rate of 40 ml/min. The data were analyzed using TA Instruments Universal Analysis 2000 software (5.5.3).

DSC measurements were performed using a TA Q200 DSC (TA Instruments–Waters LLC), with nitrogen gas as the purge at a flow rate of 50 ml/min. Approximately 5 mg of samples was placed on Tzero hermetic pans and heated from 1° to 250°C at a rate of 10°C/min. The measured data were analyzed using TA Instruments Universal Analysis 2000 software (5.5.3).

XRPD analysis

A Bruker D8 ADVANCE Powder diffractometer (Bruker) was used to assess the degree of crystallinity of the CBS-loaded or VA-loaded filaments and the corresponding powder mixtures. XRPD scans were performed in Bragg-Brentano geometry using Cu Kα radiation (λ = 1.54 Å) with a voltage of 40 kV and a current of 40 mA, using a position-sensitive detector MBraun PSD-50M. To prepare the samples for measurements, the desired filament was first ground using a fine-mill machine through a metal sieve with 1-mm pores and, subsequently, placed on the sample holder. Integration was performed over the range, from 2θ = 5° to 70° (step size, 0.0149°; 0.4 s per step).

SEM imaging

The surface and cross-section images of the filaments were determined using a JEOL JSM 7100F field emission scanning electron microscope (JEOL GmbH) in secondary electron mode. For surface imaging, samples were mounted with conductive carbon cement (Leit-C, Plano GmbH) onto 12-mm aluminum SEM stubs. For cross-section imaging, the block face of samples was smoothed using a Histo Diamond knife (DiATOME) before mounting. After the hardening of the carbon cement, rotating samples were sputter-coated with 6-nm Pt/Pd in a CCU-010 HV compact coating unit (Safematic GmbH). Images of the filament surfaces and cross sections were acquired at an accelerating voltage of 15 and 4 kV, respectively.

Mechanical properties of the filaments

A texture analyzer (TA-XT plus, Stable Micro System) was used to determine the tensile strength of the filaments. First, the filaments were cut into 50-mm-long segments and fixed vertically to the clamps of the equipment. The clamps were then stretched gradually at an elongation speed of 2 mm/s until a breaking point was observed. The stress (in megapascal) and strain (in percentage) values were calculated and plotted using Exponent software (Stable Micro Systems). The elastic modulus was calculated from the slope of the stress-versus-strain curve in the linear region. At least three replicates were performed for each type of filament.

In vitro dissolution study

The amount of CBS or VA released from the filaments and the printed prototypes was evaluated using a U.S. Pharmacopoeia dissolution apparatus 2 (paddle). For VA-loaded filaments or prototypes, a section of the filaments (approximately 200 mg) or the entire prototype was immersed in 250 ml of simulated saliva (16.8 mM Na_2HPO_4, 1.4 mM KH_2PO_4, and 137 mM NaCl; adjusted to pH 6.75) (*48*) and incubated at 37°C with a paddle rotation speed of 100 rpm. Five hundred milliliters of simulated saliva supplemented with 0.5 wt % SDS (to ensure sink conditions) was used for the dissolution studies involving CBS-loaded filaments or prototypes. At regular intervals, 200-μl aliquots of artificial saliva buffer were sampled from each flask and replaced with an equal amount of buffer. The release study was carried out for up to 14 days, and the amount of CBS or VA released was quantified by HPLC.

Scanning and 3D printing of prototypes

The oral drug delivery devices were fabricated from the filaments using a Leapfrog Xeed (Leapfrog) FDM 3D printer equipped with a dual extrusion system (nozzle diameter, 0.35 mm). An open-source CAD file for a model of teeth (https://grabcad.com/library/dental-full-contour-crown-veneer) was used for the 3D printing of a model mouthguard. Modifications to the CAD file were performed using Blender (Stichting Blender Foundation) and Autodesk Netfabb 2015 software (Autodesk Inc.) to obtain customized bilayer designs in a stereolithography (.stl) file format. Simplify3D software (Simplify3D) was used to convert .stl files to g-codes, which were subsequently exported to the printer's in-built software for printing. The two regions of the bilayered CBS-loaded mouthguards were printed at the optimized temperature of 180°C using the CBS-loaded and commercial PLA filaments. Meanwhile, the two regions of the bilayered VA-loaded mouthguards were printed at the optimized temperature of 195°C using both the VA-loaded filament and the PLA_{PG}/PVA_{PG} (9:1, w/w) filament prepared by HME. The print bed temperature was set at 45°C for both sets of prints.

For the first-in-human study, intraoral scans of the volunteers were captured using a CS 3600 intraoral scanner (Carestream), which has a powerful structured light-emitting diode light scanner to enable high-speed, continuous scanning of the maxillary anatomy. These 3D scans were then exported as .stl files that served as templates for the 3D printing of the personalized mouthguards. Before 3D printing, these templates were further optimized using various CAD software—Blender, Autodesk Netfabb, and Simplify3D. Specifically, Blender was used to increase the wall thickness of the templates. Autodesk Netfabb was used to design the models with different spatial arrangements of VA-loaded and VA-free regions and to splice the models for printing. Simplify3D was used to scale the models proportionately to obtain the best anatomical fit of the mouthguards on the individual's teeth.

All the mouthguards were fabricated in a dedicated room that had never served as a wet chemistry laboratory. All printings were performed on fresh layers of clear inkjet paper on the print bed using a brand new set of Bowden tubes and print heads and the following optimized parameters: extrusion temperature of 195°C, print bed temperature of 45°C, layer thickness of 0.15 mm, 100% rectilinear infill with support pillar resolution of 2 mm, and printing speed of 3000 mm/min. Each mouthguard required approximately 40 min for printing.

Human study

The protocol for this part of the study was approved by the Research Ethics Committee of ETH Zurich (EK 2017-N-24). Three types of personalized mouthguards comprising two designs (horizontally sliced and vertically sliced), as well as two filament blends [PVA_{PG} (high) and PVA_{PG} (low)], were printed (refer to Fig. 5A). CAD software was used to modify the mouthguards to ensure that they were of similar weight (approximately 1.3 to 1.5 g), and the initial amount of VA in all the mouthguards was controlled by setting the proportion of the VA-loaded region to exactly half of the entire mouthguard. Six volunteers (three males and three females aged 20 to 35 years) were enrolled in the study, which lasted 5 weeks in total: 3 weeks of testing separated by 2 weeks of washouts. Each volunteer tested each of the three types of mouthguard, which was worn for 2 hours per day (during which all food or drink were prohibited) for three consecutive days. The mouthguards were rinsed with denture cleaner solution prepared from Kukident tablets, followed by water for 1 min each before wearing. After each period of wearing, the mouthguard was rinsed and dried before storing in the fridge at 4°C in separate containers. A 1-week break was taken before evaluation of the next mouthguard. Saliva samples were obtained at 15-min preplacement and at predefined time intervals of 30 and 15 min after placement. The saliva (500 to 1000 μl) was collected in Eppendorf tubes without any stimulation of the salivary glands, and the tubes were vortexed and centrifuged for 5 min at 18,000*g*. Supernatants were extracted for the aforementioned HPLC analysis. After the final time point, the amount of VA remaining in the mouthguards was evaluated by HPLC. For the duration of the study, discontinuation of the study took place as soon as no further release of VA was observed or the VA was below the limit of detection.

Statistical analysis

All statistical analyses were performed using GraphPad Prism 7 software. Student's *t* test was used for all statistical analyses between two groups, while statistical analyses of more than two groups were performed using one-way analysis of variance (ANOVA) and Tukey's post hoc significance tests. To compare matched data from different groups for the human study, one-way ANOVA with the Greenhouse-Geisser correction was used.

SUPPLEMENTARY MATERIALS

Supplementary material for this article is available at http://advances.sciencemag.org/cgi/content/full/4/5/eaat2544/DC1

fig. S1. Selection of active compound and polymer blends for HME.
fig. S2. Optimization of PVA_S/PLA_S ratio for CBS-loaded filaments.
fig. S3. Thermal properties of CBS-loaded and VA-loaded filaments.
fig. S4. Characterizations of polymer mixtures containing CBS or VA.
fig. S5. Surface and cross-section of unloaded filaments.
fig. S6. Optimization of temperature for 3D printing.
fig. S7. Evaluation of the VA concentration and the weight of the mouthguards.
fig. S8. Release profiles of the personalized mouthguards in vitro.
table S1. Physicochemical properties of CBS and VA.
table S2. Feed compositions for the prepared blend filaments and the CBS loading efficiencies for the corresponding filaments.
table S3. Solubility parameter calculations of individual components of the filaments based on the Hoftyzer and Van Krevelen method and the Hoy method.
table S4. Mechanical properties of pure PLA_S filaments, pure PVA_S filaments, and the CBS-loaded blend filaments.
table S5. Mechanical properties of pure PLA_{PG}, PVA_{PG} filaments, and the VA-loaded blend filaments.
table S6. Optimization of the filament temperature and composition for the VA-free region in the mouthguard.
table S7. AUC of VA concentrations in saliva after each cycle of wearing of the three different mouthguards.
Methods
movie S1. Movie summarizing the different steps involved in the preparation of the 3D-printed compound-eluting mouthguards.
Reference (*49*, *50*)

REFERENCES AND NOTES

1. S. A. M. Tofail, E. P. Koumoulos, A. Bandyopadhyay, S. Bose, L. O'Donoghue, C. Charitidis, Additive manufacturing: Scientific and technological challenges, market uptake and opportunities. *Mater. Today* **21**, 22–37 (2018).
2. B. C. Gross, J. L. Erkal, S. Y. Lockwood, C. Chen, D. M. Spence, Evaluation of 3D printing and its potential impact on biotechnology and the chemical sciences. *Anal. Chem.* **86**, 3240–3253 (2014).
3. S. S. Robinson, S. Alaie, H. Sidoti, J. Auge, L. Baskaran, K. Avilés-Fernández, S. D. Hollenberg, R. F. Shepherd, J. K. Min, S. N. Dunham, B. Mosadegh, Patient-specific design of a soft occluder for the left atrial appendage. *Nat. Biomed. Eng.* **2**, 8–16 (2018).
4. R. J. Morrison, S. J. Hollister, M. F. Niedner, M. G. Mahani, A. H. Park, D. K. Mehta, R. G. Ohye, G. E. Green, Mitigation of tracheobronchomalacia with 3D-printed personalized medical devices in pediatric patients. *Sci. Transl. Med.* **7**, 285ra64 (2015).
5. Y. Sun, S. Soh, Printing tablets with fully customizable release profiles for personalized medicine. *Adv. Mater.* **27**, 7847–7853 (2015).
6. S. A. Khaled, J. C. Burley, M. R. Alexander, J. Yang, C. J. Roberts, 3D printing of five-in-one dose combination polypill with defined immediate and sustained release profiles. *J. Control. Release* **217**, 308–314 (2015).
7. S. E. Moulton, G. G. Wallace, 3-Dimensional (3D) fabricated polymer based drug delivery systems. *J. Control. Release* **193**, 27–34 (2014).
8. J. Norman, R. D. Madurawe, C. M. V. Moore, M. A. Khan, A. Khairuzzaman, A new chapter in pharmaceutical manufacturing: 3D-printed drug products. *Adv. Drug Deliv. Rev.* **108**, 39–50 (2017).
9. D. G. Yu, L. M. Zhu, C. J. Branford-White, X. L. Yang, Three-dimensional printing in pharmaceutics: Promises and problems. *J. Pharm. Sci.* **97**, 3666–3690 (2008).
10. M. Alhijjaj, P. Belton, S. Qi, An investigation into the use of polymer blends to improve the printability of and regulate drug release from pharmaceutical solid dispersions prepared via fused deposition modeling (FDM) 3D printing. *Eur. J. Pharm. Biopharm.* **108**, 111–125 (2016).
11. S. A. Khaled, J. C. Burley, M. R. Alexander, C. J. Roberts, Desktop 3D printing of controlled release pharmaceutical bilayer tablets. *Int. J. Pharm.* **461**, 105–111 (2014).
12. A. Goyanes, P. Robles Martinez, A. Buanz, A. W. Basit, S. Gaisford, Effect of geometry on drug release from 3D printed tablets. *Int. J. Pharm.* **494**, 657–663 (2015).
13. A. Maroni, A. Melocchi, F. Parietti, A. Foppoli, L. Zema, A. Gazzaniga, 3D printed multi-compartment capsular devices for two-pulse oral drug delivery. *J. Control. Release* **268**, 10–18 (2017).
14. N. Genina, J. P. Boetker, S. Colombo, N. Harmankaya, J. Rantanen, Anti-tuberculosis drug combination for controlled oral delivery using 3D printed compartmental dosage forms: From drug product design to in vivo testing. *J. Control. Release* **268**, 40–48 (2017).
15. M. Kyobula, A. Adedeji, M. R. Alexander, E. Saleh, R. Wildman, I. Ashcroft, P. R. Gellert, C. J. Roberts, 3D inkjet printing of tablets exploiting bespoke complex geometries for controlled and tuneable drug release. *J. Control. Release* **261**, 207–215 (2017).
16. M. Sadia, B. Arafat, W. Ahmed, R. T. Forbes, M. A. Alhnan, Channelled tablets: An innovative approach to accelerating drug release from 3D printed tablets. *J. Control. Release* **269**, 355–363 (2018).
17. First 3D-printed pill. *Nat. Biotechnol.* **33**, 1014 (2015).
18. J. Holländer, N. Genina, H. Jukarainen, M. Khajeheian, A. Rosling, E. Mäkilä, N. Sandler, Three-dimensional printed PCL-based implantable prototypes of medical devices for controlled drug delivery. *J. Pharm. Sci.* **105**, 2665–2676 (2016).
19. H.-G. Yi, Y.-J. Choi, K. S. Kang, J. M. Hong, R. G. Pati, M. N. Park, I. K. Shim, C. M. Lee, S. C. Kim, D.-W. Cho, A 3D-printed local drug delivery patch for pancreatic cancer growth suppression. *J. Control. Release* **238**, 231–241 (2016).
20. U. Gbureck, E. Vorndran, F. A. Müller, J. E. Barralet, Low temperature direct 3D printed bioceramics and biocomposites as drug release matrices. *J. Control. Release* **122**, 173–180 (2007).
21. A. Goyanes, U. Det-Amornrat, J. Wang, A. W. Basit, S. Gaisford, 3D scanning and 3D printing as innovative technologies for fabricating personalized topical drug delivery systems. *J. Control. Release* **234**, 41–48 (2016).
22. Z. Muwaffak, A. Goyanes, V. Clark, A. W. Basit, S. T. Hilton, S. Gaisford, Patient-specific 3D scanned and 3D printed antimicrobial polycaprolactone wound dressings. *Int. J. Pharm.* **527**, 161–170 (2017).
23. J. Goole, K. Amighi, 3D printing in pharmaceutics: A new tool for designing customized drug delivery systems. *Int. J. Pharm.* **499**, 376–394 (2016).

24. N. Sandler, M. Preis, Printed drug-delivery systems for improved patient treatment. *Trends Pharmacol. Sci.* **37**, 1070–1080 (2016).
25. G. H. Hildebrandt, H. R. Pape Jr., S. A. Syed, W. A. Gregory, M. Friedman, Effect of slow-release chlorhexidine mouthguards on the levels of selected salivary bacteria. *Caries Res.* **26**, 268–274 (1992).
26. M. Carbone, E. Goss, M. Carrozzo, S. Castellano, D. Conrotto, R. Broccoletti, S. Gandolfo, Systemic and topical corticosteroid treatment of oral lichen planus: A comparative study with long-term follow-up. *J. Oral Pathol. Med.* **32**, 323–329 (2003).
27. J.-P. Kruth, M. C. Leu, T. Nakagawa, Progress in additive manufacturing and rapid prototyping. *CIRP Ann. Manuf. Technol.* **47**, 525–540 (1998).
28. M. A. Alhnan, T. C. Okwuosa, M. Sadia, K.-W. Wan, W. Ahmed, B. Arafat, Emergence of 3D printed dosage forms: Opportunities and challenges. *Pharm. Res.* **33**, 1817–1832 (2016).
29. D. W. Van Krevelen, K. Te Nijenhuis, Cohesive properties and solubility, in *Properties of Polymers* (Elsevier, ed. 4, 2009), pp. 189–227.
30. C. Brough, D. A. Miller, J. M. Keen, S. A. Kucera, D. Lubda, R. O. Williams III, Use of polyvinyl alcohol as a solubility-enhancing polymer for poorly water soluble drug delivery (Part 1). *AAPS PharmSciTech* **17**, 167–179 (2016).
31. A. Goyanes, J. Wang, A. Buanz, R. Martínez-Pacheco, R. Telford, S. Gaisford, A. W. Basit, 3D printing of medicines: Engineering novel oral devices with unique design and drug release characteristics. *Mol. Pharm.* **12**, 4077–4084 (2015).
32. W. Kempin, C. Franz, L.-C. Koster, F. Schneider, M. Bogdahn, W. Weitschies, A. Seidlitz, Assessment of different polymers and drug loads for fused deposition modeling of drug loaded implants. *Eur. J. Pharm. Biopharm.* **115**, 84–93 (2017).
33. M. J. Davies, E. Costley, J. Ren, P. Gibbons, A. Kondor, M. Naderi, On drug-base incompatibilities during extrudate manufacture and fused deposition 3D printing. *J. 3D Print. Med.* **1**, 31–47 (2017).
34. C. Li, Z.-H. Wang, D.-G. Yu, G. R. Williams, Tunable biphasic drug release from ethyl cellulose nanofibers fabricated using a modified coaxial electrospinning process. *Nanoscale Res. Lett.* **9**, 258 (2014).
35. J. Zhang, X. Feng, H. Patil, R. V. Tiwari, M. A. Repka, Coupling 3D printing with hot-melt extrusion to produce controlled-release tablets. *Int. J. Pharm.* **519**, 186–197 (2017).
36. L. Perioli, V. Ambrogi, F. Angelici, M. Ricci, S. Giovagnoli, M. Capuccella, C. Rossi, Development of mucoadhesive patches for buccal administration of ibuprofen. *J. Control. Release* **99**, 73–82 (2004).
37. H. Ryokawa, Y. Miyazaki, A. Fujishima, T. Miyazaki, K. Maki, The mechanical properties of dental thermoplastic materials in a simulated intraoral environment. *Orthod. Waves* **65**, 64–72 (2006).
38. D. Tran, M. S. Cooke, P. R. H. Newsome, Laboratory evaluation of mouthguard material. *Dent. Traumatol.* **17**, 260–265 (2001).
39. R. R. Padilla, A technique for fabricating modern athletic mouthguards. *J. Calif. Dent. Assoc.* **33**, 399–408 (2005).
40. K. Nakajima, A vacuum technique to increase anterior thickness of athletic mouthguards to achieve a full-balanced occlusion. *Dent. Traumatol.* **24**, 50–52 (2008).
41. J. M. Llabot, R. H. Manzo, D. A. Allemandi, Novel mucoadhesive extended release tablets for treatment of oral candidosis: 'In vivo' evaluation of the biopharmaceutical performance. *J. Pharm. Sci.* **98**, 1871–1876 (2009).
42. R. D. Farahani, M. Dubé, D. Therriault, Three-dimensional printing of multifunctional nanocomposites: Manufacturing techniques and applications. *Adv. Mater.* **28**, 5794–5821 (2016).
43. A. Yamada, F. Niikura, K. Ikuta, A three-dimensional microfabrication system for biodegradable polymers with high resolution and biocompatibility. *J. Micromech. Microeng.* **18**, 025035 (2008).
44. B. Zhang, B. Seong, V. Nguyen, D. Byun, 3D printing of high-resolution PLA-based structures by hybrid electrohydrodynamic and fused deposition modeling techniques. *J. Micromech. Microeng.* **26**, 025015 (2016).
45. J. P. Pessan, N. S. Al-Ibrahim, M. A. R. Buzalaf, K. J. Toumba, Slow-release fluoride devices: A literature review. *J. Appl. Oral Sci.* **16**, 238–244 (2008).
46. T. C. Okwuosa, D. Stefaniak, B. Arafat, A. Isreb, K.-W. Wan, M. A. Alhnan, A lower temperature FDM 3D printing for the manufacture of patient-specific immediate release tablets. *Pharm. Res.* **33**, 2704–2712 (2016).
47. F. Mao, Q. Kong, W. Ni, X. Xu, D. Ling, Z. Lu, J. Li, Melting point distribution analysis of globally approved and discontinued drugs: A research for improving the chance of success of drug design and discovery. *ChemistryOpen* **5**, 357–368 (2016).
48. M. Jug, A. Hafner, J. Lovrić, M. L. Kregar, I. Pepić, Ž. Vanić, B. Cetina-Čižmek, J. Filipović-Grčić, An overview of in vitro dissolution/release methods for novel mucosal drug delivery systems. *J. Pharm. Biomed. Anal.* **147**, 350–366 (2018).
49. https://pubchem.ncbi.nlm.nih.gov/compound/32798.
50. https://pubchem.ncbi.nlm.nih.gov/compound/8468.

Acknowledgments: We are grateful to Carestream Dental for providing the scanning service and the image on Fig. 1A. We would also like to acknowledge F. Montalbetti for performing the preliminary tests on filament preparation and ScopeM for the experiments on SEM imaging. **Funding:** This work was financially supported by the OPO Foundation (Switzerland) and the Agency for Science, Technology and Research (Singapore). **Author contributions:** K.L., D.B., and J.-C.L. designed the experiments. K.L. and S.C. performed the experiments. All authors were involved in the analyses and interpretation of the data. K.L., D.B., and J.-C.L. wrote the manuscript. **Competing interests:** The authors declare that they have no competing interests. **Data and materials availability:** All data needed to evaluate the conclusions in the paper are present in the paper and/or the Supplementary Materials. Additional data related to this paper may be requested from the authors.

Submitted 8 February 2018
Accepted 26 March 2018
Published 9 May 2018
10.1126/sciadv.aat2544

Citation: K. Liang, S. Carmone, D. Brambilla, J.-C. Leroux, 3D printing of a wearable personalized oral delivery device: A first-in-human study. *Sci. Adv.* **4**, eaat2544 (2018).